

X-ray Study of Rekindled Accretion in the Classical Nova V2491 Cygni

Dai TAKEI,¹ Jan-Uwe NESS,² Masahiro TSUJIMOTO,³ Shunji KITAMOTO,¹ Jeremy J. DRAKE,⁴
Julian P. OSBORNE,⁵ Hiromitsu TAKAHASHI,⁶ and Kenzo KINUGASA⁷

¹*Department of Physics, Rikkyo University, 3-34-1 Nishi-Ikebukuro, Toshima, Tokyo 171-8501*
takei@ast.rikkyo.ac.jp

²*European Space Agency, XMM-Newton Observatory SOC, SRE-OAX,*
Apartado 78, 28691 Villanueva de la Cañada, Madrid, Spain

³*Japan Aerospace Exploration Agency, Institute of Space and Astronautical Science,*
3-1-1 Yoshino-dai, Chuo-ku, Sagami-hara, Kanagawa 252-5210

⁴*Smithsonian Astrophysical Observatory, MS-3, 60 Garden Street, Cambridge, MA 02138, USA*

⁵*Department of Physics & Astronomy, University of Leicester, Leicester, LE8 9DX, UK*

⁶*Hiroshima Astrophysical Science Center, Hiroshima University,*
1-3-1 Kagamiyama, Higashi-Hiroshima, Hiroshima 739-8526

⁷*Gunma Astronomical Observatory, 6860-86 Nakayama, Takayama, Agatsuma, Gunma 377-0702*

(Received 2010 November 13; accepted 2011 February 1)

Abstract

We conducted an X-ray spectroscopic study of the classical nova V2491 Cygni using our target-of-opportunity observation data with the Suzaku and XMM-Newton satellites as well as archived data with the Swift satellite. Medium-resolution ($R \sim 10\text{--}50$) spectra were obtained using the X-ray CCD spectrometers at several post-nova epochs on days 9, 29, 40, 50, and 60–150 in addition to a pre-nova interval between days –322 and –100 all relative to the time when the classical nova was spotted. We found remarkable changes in the time series of the spectra: (a) In the pre-nova phase and on day 9, the 6.7 keV emission line from FeXXV was significantly detected. (b) On day 29, no such emission line was found. (c) On day 40, the 6.7 keV emission line emerged again. (d) On days 50 and 60–150, three emission lines at 6.4, 6.7, and 7.0 keV respectively from quasi-neutral Fe, FeXXV, and FeXXVI were found. Statistically significant changes of the Fe K line intensities were confirmed between day 29 and 50. Based on these phenomena, we conclude that (1) the post-nova evolution can be divided into two different phases, (2) ejecta is responsible for the X-ray emission in the earlier phase, while rekindled accretion is for the later phase, and (3) the accretion process is considered to be reestablished as early as day 50 when the quasi-neutral Fe emission line emerged, which is a common signature of accretion from magnetic cataclysmic variables.

Key words: stars: individual (Nova Cygni 2008 number 2, V2491 Cygni) — stars: novae, cataclysmic variables — X-rays: stars

1. Introduction

A classical nova is an outburst characterized by a sudden increase in optical brightness by ~ 10 mag. It is observed in binary systems composed of a white dwarf (WD) and a main-sequence or a giant star. Hydrogen-rich material filling the Roche-lobe around the companion accretes onto the WD. When the amount of accreted material reaches a critical mass, hydrogen fusion is ignited explosively, causing a thermonuclear runaway on the WD surface (e.g., Starrfield et al. 2008). The sudden increase in radiation pressure leads to the ejection of accreted material, and a rapid and large rise in the optical brightness is observed as a classical nova. For reviews of classical novae, readers can refer to e.g., Warner (2003) and Bode & Evans (2008).

The form of mass accretion mainly depends on the strength of the magnetic field on the WD (B_{WD} ; e.g., Warner 2003). For non-magnetic or weakly magnetized WDs ($B_{\text{WD}} \lesssim 10^5$ gauss), the accretion disk is formed in

the binary system. For strongly magnetized WDs, called polars ($B_{\text{WD}} \gtrsim 10^7$ gauss), the motion of infalling material is governed by their strong magnetic field, thus instead of a disk an accretion funnel is formed along the magnetic field lines (e.g., Cropper 1990). For those with magnetic field strengths between these two, called intermediate polars (IPs), the accretion disk is truncated at the Alfvén radius where the magnetic and the ram pressures are equal to each other, from which matter accretes along the field lines (e.g., Patterson 1994). In principle, classical nova explosions can occur regardless of the strength of B_{WD} , but most observed cases are from non-magnetic or weakly magnetized WDs. Classical novae from magnetized WDs so far make up only a handful of cases (e.g., V1500 Cyg, GK Per, and CP Pup; Warner 2003; Warner 2008).

During a nova eruption, the accretion process is considered to be suspended until the radiation pressure drops at the end of nuclear processing on the WD surface (e.g., Prialnik 1986; Prialnik & Shara 1986; Shara et al. 1986). Following this, a reestablished accretion process can start

to accumulate material again for the next eruption. This typically takes a long time ($\sim 10^{4-5}$ yr), except for a handful of “recurrent” novae that undergo outbursts every ~ 10 – 100 yr (e.g., Schaefer 2010). It is currently unknown how early the accretion process resumes after a nova eruption. Drake & Orlando (2010) showed that an accretion disk can be completely destroyed in the blast. At least for the shorter period systems, a disk is expected to be rejuvenated for IPs and weakly magnetized WDs prior to accretion resumption onto the WD. The reestablishment of accretion is a key event, which affects the post-nova development and the ultimate fate of the binary system (e.g., Prialnik et al. 1982; Prialnik & Kovetz 1995). However, observations to probe rekindled accretion are difficult in the immediate aftermath of a nova, as thick material still remains around the binary system as a consequence of envelope ejection.

Moderately hard X-ray (2.0–10 keV) observations of classical novae in magnetized WDs are one of the few tools to enable direct access to rekindled accretion. X-rays can penetrate through the thick circumbinary material, allowing us to delve into the system immediately after the nova eruption. In particular, IPs emit bright X-rays of $\sim 10^{33}$ erg s $^{-1}$ in the 2.0–10 keV energy band (e.g., Chamugam et al. 1991; Norton & Watson 1989; Warner 2003), which originate from high temperature plasma produced by the accretion shock on the WD surface. Several observational methods in the moderately hard X-ray band can be used to probe the accretion process after classical novae: (1) a quasi-neutral Fe (hereafter called FeI) $K\alpha$ emission line at 6.4 keV, which is produced as fluorescence at the WD surface illuminated by hard X-ray photons of shock-excited plasma at the base of the accretion column (e.g., Ezuka & Ishida 1999), (2) flickering in the moderately hard X-ray light curve on a time scale of seconds to minutes caused by random processes in accretion (e.g., Ribeiro & Diaz 2008), and (3) X-ray periodicity due to a combination of the localized hard X-ray emission and the WD rotation (e.g., Norton & Mukai 2007).

The first method has been applied to four binary systems causing a classical nova to date. Three of them (V2487 Oph; Hernanz & Sala 2002, GK Per; Hellier & Mukai 2004, and CP Pup; Orio et al. 2009) are considered to host a magnetic WD, while the remaining one (V603 Aql; Mukai & Orio 2005) is considered to host a non-magnetic WD that is particularly bright as a nearby source at the distance of 360 pc (Hubble & Duncan 1927). The FeI $K\alpha$ fluorescent line was detected from all these samples in the post-nova phase, but the observations were made long after the outburst (~ 3 yr for V2487 Oph, ~ 60 yr for CP Pup, ~ 80 yr for V603 Aql, and ~ 100 yr for GK Per). It is thus unclear how early the accretion process was reestablished. Observations at a high cadence immediately after an outburst are obviously necessary. The second method was applied to two classical novae to date, V603 Aql (Drechsel et al. 1983) and V2491 Cyg (Page et al. 2010). In the case of V2491 Cyg, the hard X-ray light curve started to exhibit flickering no later than day 57 after the outburst, indicating that the accretion process

was reestablished at least this early. The third method has not been unambiguously reported in the post-nova evolution.

The purpose of this paper is to investigate the early reestablishment of the accretion process in V2491 Cyg (Page et al. 2010) using the FeI $K\alpha$ fluorescent line method. We assemble archived data taken at a high cadence with the Swift satellite, as well as our target-of-opportunity observations designed to obtain high signal-to-noise ratio spectra in the Fe K band (6.0–7.0 keV) at several post-nova epochs with the Suzaku and XMM-Newton satellites. The object was observed serendipitously in the pre-nova phase in X-rays (Ibarra et al. 2009), and we also aim to compare the X-ray spectra before and after the nova eruption.

The plan of this paper is as follows: In section 2, we briefly summarize the features of V2491 Cyg with ground-based and space-based observations. In section 3, we describe the X-ray observations and the data processing with the Suzaku, XMM-Newton, and Swift satellites. In section 4, we construct the X-ray spectra in the broad band (0.3–10 keV) as well as in the hard band (4.0–10 keV) around the Fe K complex at different time intervals from pre-nova to post-nova phases. We then fit the spectra with simple models to characterize line and continuum emission in the hard band. In section 5, we develop discussion to achieve the purpose mentioned above. Finally, the main results of this paper are summarized in section 6.

2. V2491 Cygni

2.1. Ground-based observations

The classical nova V2491 Cyg (Nakano et al. 2008; Samus 2008) was discovered on 2008 April 10.728 UT (54566.73 d in modified Julian date; MJD) in the constellation Cygnus at (RA, Dec) = (19^h43^m01^s.96, +32°19′13″.8) in the equinox J2000.0. We define the epoch of the discovery as the origin of time throughout this paper. V2491 Cyg is an extremely fast nova (Tomov et al. 2008b), declining at a rate of $t_2 \sim 4.6$ d (Tomov et al. 2008a) and $t_3 \sim 16.8$ d, where t_2 and t_3 are the durations to fade respectively by 2 and 3 mag from the optical maximum. The distance to V2491 Cyg was estimated to be ~ 10.5 kpc (Helton et al. 2008) using an empirical relation between the maximum magnitude and the rate of decline among classical novae (della Valle & Livio 1995).

2.2. Space-based observations

The discovery of V2491 Cyg triggered an intense monitoring campaign with Swift, which continued for more than half a year (Kuulkers et al. 2008; Osborne et al. 2008; Page et al. 2008; Page et al. 2010). Subsequent follow-up observations were also made by Suzaku and XMM-Newton. We present results from these data sets in this paper. Below, we briefly summarize other results published to date.

On day 9, Suzaku obtained an extremely flat X-ray spectrum extending up to 70 keV with a 6.7 keV emission

line from Fe XXV (Takei et al. 2009). The continuum emission was speculated to be of non-thermal origin. On days 40 and 50, XMM-Newton observations to obtain high-resolution grating X-ray spectra of the super-soft emission were made (Ness et al. 2008a; Ness et al. 2008b; Ness 2010; Ness et al. 2011). In these spectra, blackbody-like continuum emission was found, together with broad absorption lines from N VI, N VII, O VII, and O VIII as well as emission lines from Ne IX, Ne X, and Mg XII. Ness et al. (2011) found that the majority of photospheric absorption lines were blue-shifted by ~ 3000 km s $^{-1}$. Evidence for a possible X-ray periodicity of ~ 37 min was also present in the XMM-Newton light curve. Due to the low number of observed cycles, however, it is not yet certain whether this was caused by the WD rotation or red noise. If the periodicity was from rotation, it strongly suggests that the outburst originated in an IP system.

Before the outburst, Swift observed an area coincidentally including V2491 Cyg between days -322 and -100 . An X-ray source was significantly detected in five observations (Swift J194302.1+321913; Ibarra & Kuulkers 2008; Ibarra et al. 2008; Ibarra et al. 2009; Page et al. 2010), among which the spectral shape was observed to change dramatically (Ibarra et al. 2009). At the position of V2491 Cyg, X-ray emission was also detected in the ROSAT all-sky survey faint source catalogue (1RXS J194259.9+321940; Voges et al. 2000), the second ROSAT PSPC catalogue¹ (2RXP J194302.0+321912), and the XMM-Newton slew survey catalogue (XMMSL1 J194301.9+321911; Saxton et al. 2008). This makes V2491 Cyg one of the few examples of classical novae with an X-ray detection prior to outburst. The pre-nova X-ray activity suggests that it hosts a magnetic WD (Ibarra et al. 2009).

3. Observations and reduction

3.1. Suzaku

Following the X-ray detection by Swift during monitoring of the nova, we made two target-of-opportunity observations using the Suzaku satellite on 2008 April 19 and May 9 (days 9 and 29; table 1 and figure 1). Suzaku has two instruments in operation (Mitsuda et al. 2007): the X-ray Imaging Spectrometer (XIS; Koyama et al. 2007) and the Hard X-ray Detector (HXD; Takahashi et al. 2007; Kokubun et al. 2007). The observations were aimed so as to put V2491 Cyg at the XIS field center with different roll angles. Part of the data from the first observation, emphasizing the HXD spectrum, was reported in Takei et al. (2009). In this paper, we concentrate on the XIS data from both observations, focusing on the Fe K band.

The XIS is equipped with four X-ray CCDs at the foci of four X-ray telescope modules (Serlemitsos et al. 2007). Three of them (XIS0, 2, and 3) are front-illuminated (FI) CCDs sensitive in a 0.4–12 keV energy range. The remaining one (XIS1) is a back-illuminated (BI) CCD sensitive

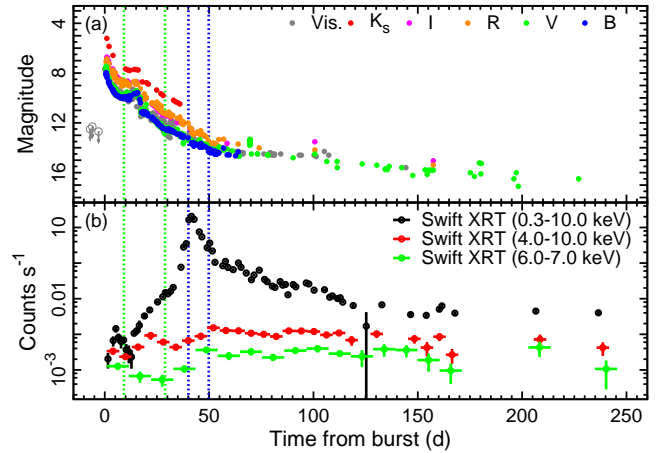


Fig. 1. Development of the (a) optical and (b) X-ray brightness of V2491 Cyg. The origin of the abscissa is 54566.73 d (MJD) when the classical nova was spotted (Nakano et al. 2008). The time of the Suzaku and XMM-Newton observations are indicated by dotted lines with green and blue colors, respectively. (a) The *B*-, *V*-, *R*-, *I*-, *Ks*-band, and visual magnitudes are shown with different colors. The upper limit for visual magnitudes before the outburst (Nakano et al. 2008) is indicated by open circles and arrows. (b) The background-subtracted X-ray count rates from Swift in the broad band (0.3–10 keV), the hard band (4.0–10 keV), and the Fe K band (6.0–7.0 keV) with different colors. The optical photometry data are taken from the American Association of Variable Star Observers (AAVSO), the Variable Star Observers League in Japan (VSOLJ), and other ground-based observations (Nakano et al. 2008; Lynch et al. 2008; Ashok et al. 2008; Tomov et al. 2008b; Tomov et al. 2008a; Rudy et al. 2008; Helton et al. 2008). The infra-red photometry data were obtained by the Kanata TRISPEC team².

at 0.2–12 keV. As of the observation dates, the absolute energy scale is accurate to $\lesssim 10$ eV, the energy resolution is 160–190 eV (FWHM) at 5.9 keV, and the total effective area is ~ 400 cm 2 at 8 keV. Each XIS has a format of 1024 \times 1024 pixels and covers a 18' \times 18' field of view with an energy-independent half-power diameter of 1'8–2'3. XIS2 has not been functional since 2006 November, thus we used the remaining three CCDs in our observations. The XIS was operated in the normal clocking mode with a frame time of 8 s. The spaced-row charge injection technique (Nakajima et al. 2008) were employed for the XIS to rejuvenate its spectral resolution by filling the charge traps with artificially injected electrons through CCD readouts.

The data were processed with the pipeline version 2.2.7.18, in which events were removed during the South Atlantic anomaly passages, the night earth elevation angles below 5°, and the day earth elevation angles below 20°. For data reduction, we used the High Energy Astrophysics Software (HEASoft) package³ version 6.6.2 and the calibration database version hxd20080201_xis20080201_xrt20070622_xrs20060410. As a result, the net exposure times of ~ 21 and ~ 25 ks were obtained for days 9 and 29, respectively.

¹ <http://www.xray.mpe.mpg.de/rosat/rra/rospspc/>

² <http://kanatatmp.g.hatena.ne.jp/>

³ <http://heasarc.gsfc.nasa.gov/docs/software/lheasoft/>

Table 1. List of our target-of-opportunity observations.

Mission/Detector	Obs ID	Start time (UT)	End time (UT)	t^* (d)	Δt^\dagger (ks)	Count rate ‡ (s $^{-1}$)
Suzaku/XIS	903001010	2008-04-19 15:21	2008-04-20 02:00	9.13	21	0.02
	903001020	2008-05-09 08:39	2008-05-09 21:30	28.90	25	0.20
XMM-Newton/EPIC-PN	0552270501	2008-05-20 14:24	2008-05-21 00:58	40.09	29	212.0
	0552270601	2008-05-30 08:41	2008-05-30 17:05	49.81	27	38.4

* Elapsed days in the middle of the observation from the discovery of V2491 Cyg (54566.73 d in MJD; Nakano et al. 2008).

† Net exposure time averaged over the operating CCDs.

‡ The background-subtracted count rate in the 0.3–10 keV energy band over the operating CCDs.

3.2. XMM-Newton

Following the flux increase in the soft X-ray band about a month after the nova outburst, two target-of-opportunity observations were carried out using the XMM-Newton satellite on 2008 May 20 and 30 (days 40 and 50; table 1 and figure 1). XMM-Newton has three instruments in operation (Jansen et al. 2001): the European Photon Imaging Camera (EPIC; Strüder et al. 2001; Turner et al. 2001), the Reflection Grating Spectrometer (RGS; den Herder et al. 2001), and the Optical Monitor (OM; Mason et al. 2001; Talavera 2009). The results obtained from the RGS data can be found in Ness et al. (2008a), Ness et al. (2008b), Ness (2010), and Ness et al. (2011). In this paper, we concentrate on the EPIC data, focusing on the Fe K band.

The EPIC is equipped with three X-ray CCD arrays at the foci of three X-ray telescopes. Two of them use MOS-type CCDs (EPIC-MOS; Turner et al. 2001) sensitive in the 0.15–12 keV energy range, and the remaining one employs a PN-type CCD (EPIC-PN; Strüder et al. 2001) sensitive at 0.15–15 keV. The EPIC-MOS was operated in the small window mode, while the EPIC-PN was in the timing mode. We do not use the EPIC-MOS spectra of V2491 Cyg here for the following reasons: (1) they suffered severe pile-up, and (2) a lower signal-to-noise dataset resulted because of the smaller effective area than that of the EPIC-PN by a factor of ~ 4 at the Fe K band. Annulus source extraction does not work to mitigate the pile-up issue in this case; the pile-up is caused by intense soft X-ray band emission and it is difficult to obtain a sufficiently strong signal for the fainter, harder emission in annular regions.

In the timing mode of the EPIC-PN, only a part of the CCD number 4 in the array is read out in continuous clocking to mitigate pile-up. As a consequence, a one dimensional (64 \times 1 pixels) image is obtained. The half-power diameter of the X-ray telescope is $\sim 15''$, which corresponds to 4 pixels. The absolute energy scale is accurate to ~ 50 eV at Fe K band, the energy resolution is ~ 150 eV (FWHM) at 6.4 keV (Guainazzi et al. 2010), and the effective area is ~ 600 cm 2 at 8 keV.

We used the Science Analysis Software (SAS)⁴ version 8.0.0 in data reduction. In the background light curve constructed using the 10–12 keV energy band events, several spikes were recognized as flares. We removed events

taken during these flare intervals. The intervals were defined as time bins with background count rates of more than 0.36 and 0.95 s $^{-1}$, respectively, for the observations on days 40 and 50. These criteria were derived using a recursive clipping algorithm (e.g., Maughan et al. 2004) to remove time bins having more background counts than the average by 3σ . As a result, net exposure times of ~ 29 and ~ 27 ks were obtained for days 40 and 50, respectively.

3.3. Swift

We retrieved the archived data taken by the Swift satellite both before and after the outburst. Swift has three instruments in operation (Gehrels et al. 2004): the Burst Alert Telescope (BAT; Barthelmy et al. 2005), the X-Ray Telescope (XRT; Burrows et al. 2005) and the Ultraviolet and Optical Telescope (UVOT; Roming et al. 2005). The XRT and UVOT results were presented in Page et al. (2010) and Ibarra et al. (2009) for the post-nova and pre-nova data, respectively. We reanalyze the XRT data focusing on the Fe K band in this paper.

The XRT is equipped with an X-ray CCD at the focus of an X-ray mirror module. The chip has a format of 600 \times 600 pixels covering a 23.6 \times 23.6 field of view at a telescope half-power diameter of $\sim 18''$. The device is sensitive in the range 0.3–10 keV, with an energy resolution of ~ 180 eV (FWHM) at 5.9 keV as of the observation dates. The effective area is ~ 20 cm 2 at 8 keV (Mukerjee et al. 2004). The XRT was operated in the state that selects the clocking mode automatically depending on the source count rate. The present data were mainly taken with the Photon Counting (PC) and the Windowed Timing (WT) modes. The PC mode provides full imaging and spectroscopic resolution with a frame time of 2.5 s, while the WT mode provides a one dimensional stacked image using the central 200 \times 10 pixels in continuous clocking.

For data reduction, we used the HEASoft package³ version 6.9 and the calibration database version b20070924_u20071106_x20071101_m20071023. The data were processed using the `xrtpipeline` tool to produce level 2 event files with standard screening criteria. As a result, total net exposure times of ~ 18 ks and ~ 185 ks were obtained in the pre-nova and post-nova phases.

⁴ <http://xmm.esac.esa.int/sas/>

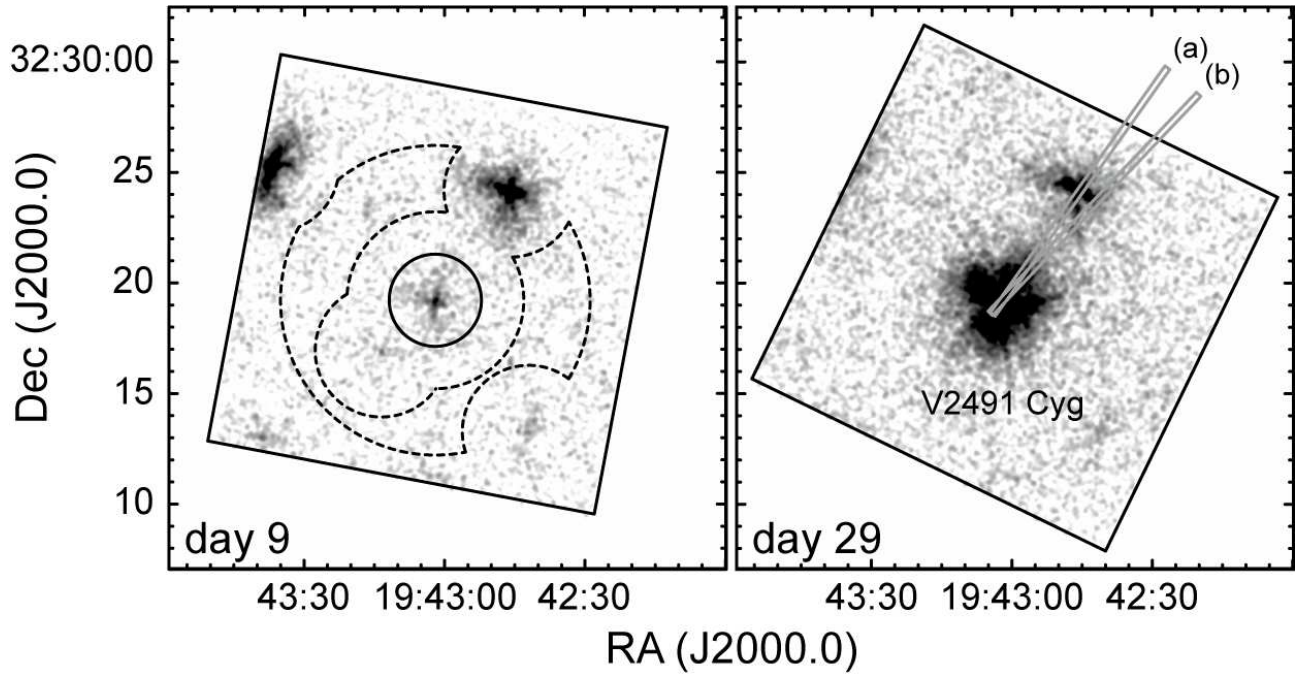


Fig. 2. Smoothed Suzaku XIS images of V2491 Cyg on days 9 and 29. Events recorded by the three CCDs in the 0.2–12 keV range were used, excluding those in the 5.0–7.0 keV range to eliminate the signals from the calibration sources at the corners. In the left panel, the XIS source extraction region is shown as a solid circle, while the background extraction region is shown using dashed lines. In the right panel, the source extraction regions for the EPIC-PN data are shown for days (a) 40 and (b) 50 as gray rectangles.

4. Analysis

4.1. Constructing spectra and light curves

4.1.1. Suzaku

Figure 2 shows the smoothed XIS image in the 0.2–12 keV energy band obtained on days 9 and 29. The astrometry of the XIS images were registered by matching the position of V2491 Cyg with that by the optical observation (Nakano et al. 2008). The source events were accumulated from a circle with a radius of 120 pixels ($2'1''$) to maximize the signal-to-noise ratio (solid circle in figure 2), while the background events were from an annulus region with inner and outer radii of $4'$ and $7'$, respectively. We masked $3'$ radius circles around other detected sources in the background region.

The background-subtracted XIS spectra were constructed separately for days 9 and 29. Figure 3 shows the broad-band (0.3–10 keV) spectra, while figure 4 shows the narrow-band (6.0–8.0 keV) spectra around the Fe K complex. The detector and mirror responses were generated using the `xisrmfgen` and `xissimarfgen` tools (Ishisaki et al. 2007), respectively. The two XIS-FI spectra with nearly identical responses were merged, while the XIS-BI spectrum was treated separately. The difference in the effective area due to different off-axis angles were compensated between source and background regions using a method described in Hyodo et al. (2008). The fraction of photon pile-up is negligible ($\lesssim 0.1\%$) in both observations.

4.1.2. XMM-Newton

In the one dimensional image of the EPIC-PN data obtained in the timing mode, V2491 Cyg is centered near

columns 36–37. The source events were accumulated from columns 35–38, while the background events were from columns 3–4 and 61–62. We show background-subtracted spectra both in the broad band (0.3–10 keV) and the narrow band (6.0–8.0 keV) separately for days 40 and 50 (figures 3 and 4, respectively). The detector and mirror responses were generated using standard SAS tools.

The V2491 Cyg spectrum on day 40 was unfortunately contaminated by a nearby source in the source region (figure 2). In the timing mode data, the image is stacked in the readout direction, so their overlapping signals cannot be separated. Therefore, we extracted the EPIC-MOS spectrum from the contaminating source and evaluated the level of contamination. The hard-band (4.0–10 keV) spectrum was fitted by a power-law model, and a statistically-acceptable fit was obtained for a photon index of 1.5 ± 0.7 and an X-ray flux of $(7.6 \pm 1.5) \times 10^{-13}$ erg cm $^{-2}$ s $^{-1}$ (90% statistical uncertainty). We show the contribution of the nearby source for the V2491 Cyg spectrum on day 40 in figure 3 and 4, in which we normalized the spectrum of the contaminating source by taking into account the reduced effective area at an off-axis position. The X-ray flux of the contamination source was estimated to be comparable with that of V2491 Cyg in the hard band (4.0–10 keV). We checked all data sets from Suzaku, XMM-Newton, and Swift observations, and no emission line was detected in the Fe K band. Therefore, the emission line in the V2491 Cyg spectrum on day 40 is entirely attributable to V2491 Cyg itself. Hereafter, we remove the contamination by including the best-fit model of the contaminating source in the spectral fitting of V2491 Cyg

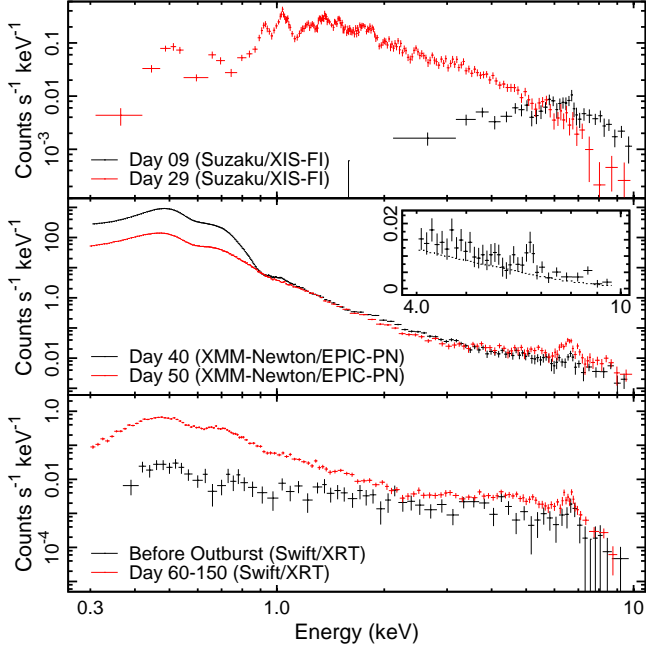


Fig. 3. Background-subtracted broad-band (0.3–10 keV) X-ray spectra of V2491 Cyg at six different epochs. The top, middle, and bottom panels show the spectra with Suzaku/XIS-FI, XMM-Newton/EPIC-PN, and Swift/XRT, respectively. The contamination by the nearby source in the XMM-Newton/EPIC-PN spectra on day 40 is shown as the dotted line in the inset of the middle panel.

on day 40. We note here that the signals of V2491 Cyg and the contamination source on day 50 can be clearly separated in the one dimensional image with different roll angles.

4.1.3. *Swift*

For the XRT data, the source events were accumulated from a circle with a radius of 20 pixels ($47''$), while the background events were from an annulus with inner and outer radii of 50 and 70 pixels ($118''$ and $165''$), respectively. For several data sets largely affected by photon pile-up, we masked the core in the source extraction circle. The core radii were adaptively chosen to extract the source event with a pile-up fraction of less than 1% for each snapshot observation. The light curves were constructed in the broad band (0.3–10 keV), the hard band (4.0–10 keV), and the Fe K band (6.0–7.0 keV), which are shown in figure 1. We grouped several snapshot observations for each epoch. The telescope vignetting, the reduced aperture due to pile-up masking and bad pixels were taken into account for the aperture photometry.

In order to investigate the spectral development with sufficient photon statistics in the Fe K band, we stacked the pre-nova data between days -322 and -100 into one spectrum and the post-nova data between days 60 and 150 into another, upon confirmation that there is no significant change in the 6.0–7.0 keV light curve. The PC mode data were used for this purpose to ensure sufficient energy resolution to resolve the three Fe emission lines. We made the broad-band and the narrow-band spectra, which are illustrated in figures 3 and 4 respectively for the pre-nova

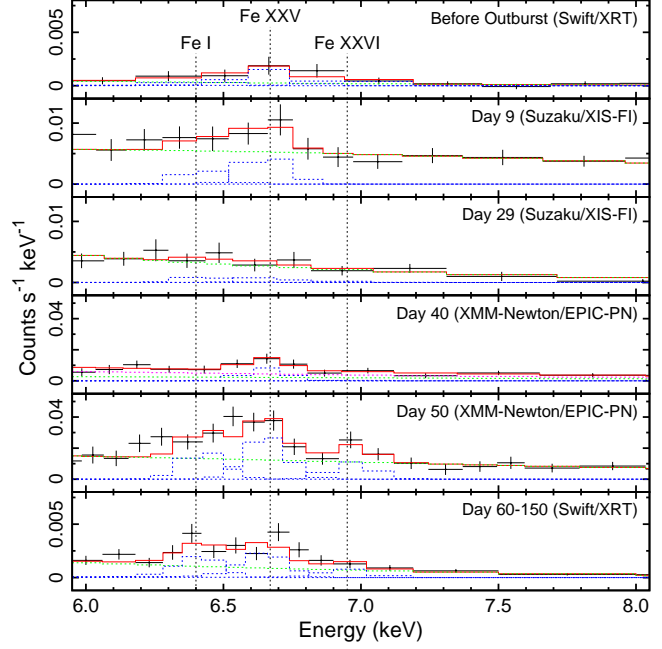


Fig. 4. Background-subtracted narrow-band (6.0–8.0 keV) X-ray spectra of V2491 Cyg, including the Fe K complex, at six different epochs. The center energy of the three emission lines are indicated by dashed lines. Black pluses indicate the data, while the red solid histograms indicate the best-fit model. The model is decomposed into the power-law continuum (green dotted) and the three Gaussian line (blue dotted) components. The contamination by the nearby source in the XMM-Newton/EPIC-PN spectra on day 40 is shown as the dotted line in magenta.

and the post-nova phases.

4.2. *Spectral Modeling*

4.2.1. *Phenomenological fitting*

We first characterize line emission in the hard-band (4.0–10 keV) spectra. For identifying the three lines in the Fe K complex (figure 4), we fitted the hard-band (4.0–10 keV) spectra using a phenomenological model composed of a power-law continuum and three Gaussian line components. The Gaussian energy of each line was tied among the six different spectra such that the line energies were not allowed to vary between them. The Gaussian width was fixed to zero for all lines for all spectra: as the expected width is negligible compared with the instrumental resolution. Other parameters were allowed to vary independently for each spectrum.

We obtained statistically acceptable results for the fitting, with the null hypothesis probability for the χ^2 value of >0.05 . The best-fit energy centers for the three Gaussian components are 6.42 ± 0.08 , 6.66 ± 0.04 , and 6.96 ± 0.08 keV (90% statistical uncertainty), which are consistent respectively with the energies of the $K\alpha$ fluorescent line from Fe I, the $1s^1S_0-2p^1P_1$ resonance line from Fe XXV, and the $Ly\alpha$ line from Fe XXVI. The flux and the equivalent width of each emission line are tabulated in table 2, in which 90% upper limits are given for undetected lines. The development of the Fe K line intensities is also

Table 2. Best-fit parameter values from the phenomenological line fitting*.

t^\dagger (d)	Flux (10^{-6} photons $\text{cm}^{-2} \text{s}^{-1}$)			Equivalent width (10^2 eV)		
	Fe I	Fe XXV	Fe XXVI	Fe I	Fe XXV	Fe XXVI
$\{-322, -100\}^\ddagger$	< 9.5	10.4 (2.1–18.5)	< 13.7	< 7.9	5.0 (0.6–17.7)	< 13.3
9.13	< 2.6	2.6 (1.1–4.2)	< 1.0	< 1.7	1.7 (0.5–2.9)	< 1.7
28.90	< 1.5	< 1.5	< 1.1	< 2.3	< 2.3	< 2.9
40.09 [§]	< 1.3	3.0 (1.4–4.6)	< 1.6	< 3.5	6.9 (2.0–11.4)	< 4.0
49.81	6.3 (3.6–9.4)	10.1 (6.9–13.0)	4.3 (1.7–7.0)	1.6 (0.9–2.4)	2.6 (1.8–3.7)	1.2 (0.4–2.2)
$\{60, 150\}^\ddagger$	10.2 (5.8–14.3)	13.3 (8.4–19.1)	5.4 (1.7–9.2)	2.3 (1.2–3.7)	3.0 (1.8–4.9)	1.4 (0.4–2.9)

* The statistical uncertainties and upper limits indicate the 90% confidence ranges.

[†] Elapsed days from the discovery of V2491 Cyg (54566.73 d in MJD; Nakano et al. 2008).

[‡] The time {X, Y} indicates the time interval between days X and Y.

[§] Increased uncertainty due to the contaminating source is not included.

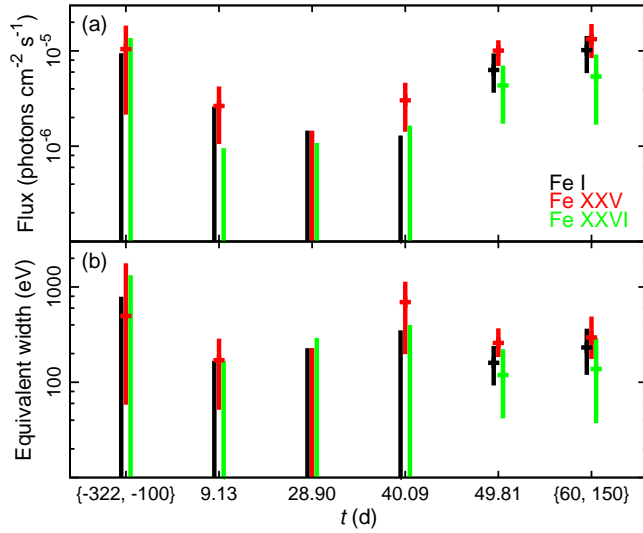


Fig. 5. Development of the (a) flux and (b) equivalent width of Fe I (black), Fe XXV (red), and Fe XXVI emission lines. The best-fit values and 90% confidence ranges are shown at six different epochs. Increased uncertainty due to the contaminating source on day 40 is not included.

shown in figure 5. The flux and the equivalent width on day 40 are subject to further uncertainty due to the propagated uncertainty from the fitting of the contaminating source, which is estimated as 2×10^{-7} photons $\text{cm}^{-2} \text{s}^{-1}$ and 300 eV, respectively.

4.2.2. Plasma model fitting

We next characterize the continuum and line emission using a thermal plasma emission model. We fitted the hard-band (4.0–10 keV) spectra using an optically-thin isothermal plasma component (APEC; Smith et al. 2001). This plasma component accounts for the continuum as well as the emission lines from highly ionized Fe and other metals. We fixed the chemical abundance to be solar (Anders & Grevesse 1989) for all the elements other than Fe for all the six different spectra. A narrow Gaussian component accounting for the 6.4 keV emission line due to the Fe fluorescence was also included. The combined model was multiplied with an interstellar absorption model (TBabs; Wilms et al. 2000). The X-ray spectrum on day 9 was excluded from the plasma model

analysis due to severe contamination by non-thermal emission of V2491 Cyg that renders diagnosis of the softer thermal component difficult. For fitting results for the data on day 9 using both plasma and non-thermal models, see Takei et al. (2009).

We obtained statistically acceptable results for all the fitting. The best-fit plasma temperature ($k_B T$), the Fe abundance relative to solar (Z_{Fe}), the detected X-ray flux (F_X), and the absorption-corrected luminosity (L_X) in the hard band (4.0–10 keV) are summarized in table 3. A distance of 10.5 kpc was assumed (Helton et al. 2008). The absorption column density (N_H) was fixed to be $2.2 \times 10^{21} \text{ cm}^{-2}$ based on the analysis of the quiescent phase data by Ibarra et al. (2009). By extrapolating the best-fit model, we estimated the X-ray luminosity in the 2.0–10 keV energy band to be in the order of $\sim 10^{34} \text{ erg s}^{-1}$. The fitting results on day 40 are again subject to increased uncertainty in the fitting uncertainty of the contaminating source. It is estimated that ± 1.5 keV in $k_B T$, ± 2.5 solar in Z_{Fe} , $\pm 1.0 \times 10^{-13} \text{ erg cm}^{-2} \text{s}^{-1}$ in F_X , and $1.3 \times 10^{33} \text{ erg s}^{-1}$ in L_X .

5. Discussion

5.1. Phases of X-ray emission

V2491 Cyg shows completely different light curves for the soft and hard parts of the X-ray band (figure 1; see also figures 1 and 4 in Page et al. 2010). The soft-band flux was negligible immediately after the outburst, but continued to increase to reach a peak at day ~ 40 , then faded rapidly until day ~ 50 and more slowly thereafter. This behavior is commonly seen in the soft X-ray light curves of other classical novae. The increase in soft-band brightness before the peak is interpreted in terms of an increasing plasma temperature (e.g., Osborne et al. 2011) and/or a decreasing extinction column as the ejecta expands, while the decrease in brightness after the peak is interpreted as the shrinkage of the photosphere after the fuel, in the form of H-rich accreted material, is consumed.

In contrast to the soft band, the hard-band light curve is relatively stable (figure 1; see also figures 1 and 4 in Page et al. 2010). Despite the overall stability, however, we argue that the hard-band development can be divided into two phases (earlier and later phases hereafter) separated

Table 3. Best-fit parameter values from plasma model fitting*.

t^\dagger (d)	$k_B T$ (keV)	Z_{Fe} (solar)	F_X^\ddagger (10^{-13} erg cm $^{-2}$ s $^{-1}$)	$L_X^{\ddagger\S}$ (10^{33} erg s $^{-1}$)	χ_{red}^2 (d.o.f.)
$\{-322, -100\}^\parallel$	7.6 (3.0–18.2)	2.6 (0.8–7.0)	7.5 (2.1–9.2)	9.9 (2.8–12.2)	0.54 (16)
9.13	(Plasma fitting omitted estimate because of dominant continuum from non-thermal emission.)				
28.90	2.1 (1.7–2.6)	< 0.1	5.5 (4.0–5.8)	7.3 (5.3–7.7)	0.77 (45)
40.09 [#]	6.2 (3.0–10.9)	1.3 (0.5–2.7)	2.5 (0.4–3.2)	3.3 (0.6–4.2)	0.65 (32)
49.81	9.6 (7.9–12.2)	1.4 (1.0–1.8)	14.3 (12.8–15.3)	18.9 (17.0–20.3)	1.34 (37)
$\{60, 150\}^\parallel$	7.3 (5.5–9.5)	1.1 (0.8–1.6)	16.7 (14.5–17.9)	22.2 (19.3–23.8)	0.65 (30)

* The statistical uncertainties and upper limits indicate the 90% confidence ranges.

† Elapsed days from the discovery of V2491 Cyg (54566.73 d in MJD; Nakano et al. 2008).

‡ These values are derived in the 4.0–10 keV energy band.

§ A distance of 10.5 kpc (Helton et al. 2008) is assumed for the luminosity.

$^\parallel$ The time {X, Y} indicates the time interval between days X and Y.

[#] Increased uncertainty due to the contaminating source is not included.

at day ~ 40 based on the following lines of evidence: (1) In the Fe K band light curve (figure 1), the flux changes gradually in the earlier phase with a minimum on day ~ 30 , whereas the flux is stable in the later phase. (2) In the narrow-band spectra (figure 4), the Fe I K α fluorescent line at 6.4 keV is only detected with a significance greater than the $3\text{-}\sigma$ level in the later phase (figure 5). (3) In the plasma model fitting results (table 3), the Fe abundance relative to H is different between the two phases. In the earlier phase, a stringent upper limit to the Fe abundance was obtained for the spectra on day 29 of $Z_{\text{Fe}} < 0.1$, which is reasonable from the lack of 6.7 keV lines despite the plasma temperature (~ 2.1 keV) being close to the maximum formation temperature of the line (e.g., Rothenflug & Arnaud 1985). In the later phase, the two lines from highly ionized Fe are clearly detected (figure 4) with a corresponding Fe abundance of $Z_{\text{Fe}} \sim 1$. Here, we note that the Fe abundance values are subject to change with the unconstrained chemical composition of other elements, which contribute to continuum emission in the X-ray band. However, we consider that the comparative values between two different spectra are valid as long as the chemical abundance of the plasma is assumed to be the same.

5.2. Origins of the X-ray emission

The two distinctive phases in the hard-band evolution of V2491 Cyg suggest that there are two different production mechanisms operating in each phase. We consider that plasma generated by shocks in the ejecta is responsible for the earlier phase, while emission by accretion shocks in the rekindled accretion process is responsible for the later phase.

Hard components from classical novae were first reported in V838 Her (Lloyd et al. 1992). Such hard emission has been established as a common phenomenon among classical novae by recent intensive monitoring observations with Swift (e.g., Bode et al. 2006; Ness et al. 2009; Page et al. 2009; Page et al. 2010; Osborne et al. 2011) and subsequent follow-up observations with XMM-Newton, Suzaku, and others (e.g., Sokoloski et al. 2006; Nelson et al. 2008; Tsujimoto et al. 2009). Viable in-

terpretations for the hard components include the plasma produced by internal shocks; i.e., ejecta with different velocities collide with each other (Friedjung 1987; Mukai & Ishida 2001). The X-ray spectra are represented by optically-thin thermal plasma emission with a plasma temperature of several keV (e.g., Lloyd et al. 1992; Mukai & Ishida 2001; Orio et al. 2001; Tsujimoto et al. 2009). For unknown reasons, Fe is often depleted in the chemical composition (e.g., V382 Vel; Orio et al. 2001, V458 Vul; Tsujimoto et al. 2009). These features are quite similar to those found in the hard component in the earlier phase of V2491 Cyg.

On the other hand, the hard component in the later phase is more similar to that commonly seen in IPs. The defining characteristics of IP X-ray emission include the following (e.g., Ezuka & Ishida 1999): (1) The Fe emission lines are clearly seen at 6.4, 6.7, and 7.0 keV respectively from Fe I, Fe XXV, and Fe XXVI. (2) The continuum emission is very flat, which is represented by thermal bremsstrahlung of a temperature of ~ 10 keV. (3) The X-ray luminosity in the 2.0–10 keV energy band is $\sim 10^{33}$ erg s $^{-1}$ (e.g., Chanmugam et al. 1991; Norton & Watson 1989; Warner 2003), which is much brighter than that of non-magnetic or weakly magnetized WDs and polars (e.g., Mukai & Shiokawa 1993; Warner 2003; Baskill et al. 2005; Byckling et al. 2010). The hard-band luminosity of V2491 Cyg ($\sim 10^{34}$ erg s $^{-1}$) is even larger than the typical IPs. This may be due to a higher accretion rate in the system. (4) The harder band (> 2 keV) emission dominates the spectrum in IPs. In contrast, the softer band (< 2 keV) emission dominates the spectrum in polars. (5) The modulation due to the WD spin and orbital motions are shown in the X-ray light curve (see Ness et al. 2011 for results of the timing analysis for V2491 Cyg). In IPs, the high temperature plasma responsible for the flat continuum and the highly ionized Fe lines is caused by a shock at the base of the accretion funnel. The plasma illuminates the WD surface, which produces a prominent Fe I K α fluorescent line. All these features are seen in the hard-band emission in the later phase of V2491 Cyg.

It is important to note three things in the results. The first is the equivalent width of the Fe I line found in the

later phase. The observed equivalent width ($\gtrsim 100$ eV) is comparable to those observed in IPs (e.g., Ezuka & Ishida 1999). It can be explained by fluorescence at the WD surface, or at the surface of the accretion disk, by X-ray emitting plasma at the base of the accretion funnel in the proximity of the WD (e.g., Ishida et al. 1991; George & Fabian 1991). It corresponds to the “infinite plane” fluorescence included in the calculations by Drake et al. (2008). However, such a large equivalent width cannot be explained for cases in which (1) the plasma heated by ejecta shocks illuminates the WD surface, or (2) the plasma heated by ejecta or accretion shocks illuminates cold material in the ejecta. In case (1), the subtended angle of the WD surface is too small ($\Delta\Omega/4\pi \sim 10^{-12}$, assuming that the X-ray emitting region has expanded for 50 d at a constant speed of 3000 km s^{-1}). In case (2), the cold material is too thin to produce the Fe fluorescence with a large equivalent width. Although the cold matter subtends the entire sphere (4π steradian), the ejecta with a hydrogen column density of $\sim 10^{21} \text{ cm}^{-2}$ (Page et al. 2010) can yield the equivalent width of only $\lesssim 10$ eV for ~ 10 keV thermal plasma X-rays (see equation 4 in Tsujimoto et al. 2005). This is in line with our interpretation that the hard component in the later phase is from the accretion process in the WD.

The second is that the hard-band features in the pre-nova phase of V2491 Cyg resemble those in the later phase of the post-nova spectra more than those in the earlier phase regarding the presence of Fe emission lines (figure 4) and the spectral hardness (table 3). This suggests that the origin of dominant X-ray emission is the same between the pre-nova and the later post-nova phases. A notable difference can be found in the hard-band flux. It is significantly higher in the late post-nova phase after day 50 than in the pre-nova phase. We speculate that the accretion rate in the late post-nova phase may have been higher than that in the pre-nova phase, which might be expected due to the heating of the secondary star by the outburst and the heated WD (Schaefer & Collazzi 2010).

The third is that V2487 Oph (Hernanz & Sala 2002), GK Per (Hellier & Mukai 2004), and CP Pup (Orio et al. 2009), which are the other three among four classical novae with a FeI fluorescence detection in the post-nova phase, also share characteristics with IPs such as high X-ray luminosity in the quiescent phase (e.g., Cordova et al. 1981; Balman et al. 1995; Hernanz & Sala 2002) and the rapidity of the optical decline (t_3 is ~ 8 d for V2487 Oph; Liller & Jones 1999; Pagnotta et al. 2009, ~ 13 d for GK Per; Downes & Duerbeck 2000, and ~ 6.5 d for CP Pup; Payne-Gaposchkin 1957; Orio et al. 2009).

5.3. Time-scale of accretion reestablishment

Using the Fe emission lines, we argued that the accretion process in V2491 Cyg was reestablished by at least ~ 50 days after the outburst. Page et al. (2010) argued that the accretion was rekindled no later than day 57 using the X-ray flux flickering method. These independent methods lead to the same conclusion on the time scale for the accretion process to resume after the nova.

The time for the reestablishment of the accretion process coincides with the time when the soft-band emission starts to decline (figure 1). This is consistent with the following scenario. The accretion disk was likely destroyed by the blast (Drake & Orlando 2010). Immediately after the outburst, the strong radiation pressure inhibits rejuvenation of the accretion disk and likely exceeds the ram pressure of the accretion flow once reestablished, thereby preventing accretion to occur. When the H-rich fuel had been consumed on the WD surface by nuclear burning and the radiation pressure started to drop, the accretion resumed. We further speculate that the magnetic field on the WD is responsible for the short time scale of rekindled accretion. When mass accretion from the companion star was switched on after a post-nova interval, the viscous time scale of the accretion disk would have to elapse before gas could again reach the WD surface (e.g., Frank et al. 1992). For a magnetized WD, accretion could resume earlier as less disk spreading is required. The scenario will be tested by examining the coincidence of the decline in the soft-band flux and the emergence of the FeI emission line by high-cadence X-ray observations of classical novae in the future.

6. Summary

We conducted a spectroscopic study of the classical nova V2491 Cyg in the hard X-ray band (4.0–10 keV) using our target-of-opportunity Suzaku and XMM-Newton data, as well as archived Swift data. X-ray spectra were obtained at five post-nova epochs on days 9, 29, 40, 50, and 60–150, in addition to a pre-nova interval between days -322 and -100 . In the time series of the spectra, we found remarkable changes in the X-ray emission: (a) In the pre-nova phase and on day 9, the 6.7 keV emission line from Fe XXV was significantly detected. The pre-nova spectra represented thermal plasma emission with an Fe abundance of 0.8–7.0 solar. (b) On day 29, no Fe lines were detected in the spectra. The Fe abundance of the dominant emission was constrained to be less than 0.1 solar. (c) On day 40, the 6.7 keV emission line was detected again. (d) In a later phase, three emission lines at 6.4, 6.7, and 7.0 keV from Fe I, Fe XXV, Fe XXVI, respectively, were found in the spectra. The Fe abundance and the flux in the hard X-ray band were significantly larger than those of the earlier phase. We also confirmed the long-term behavior of X-ray emission in the Fe K band (6.0–7.0 keV), in which the flux changes gradually in the earlier phase with a minimum on day ~ 30 and it is stable in the later phase.

Based on these results, we conclude that (1) the post-nova evolution in the X-ray light curve can be divided into two different phases separated at day ~ 40 , (2) it is most likely that shocks within the nova ejecta are responsible for the X-ray emission in the earlier phase, while shocks in the rekindled accretion are responsible for the later phase X-rays, and (3) the accretion process is considered to be reestablished by at least day ~ 50 when the FeI emission line emerged, which is a common feature for accretion

shock emission from IPs.

The authors appreciate the reviewer for useful suggestions. The authors also thank the Suzaku and XMM-Newton telescope managers for allocating telescope times for our target-of-opportunity programs. D.T. expresses gratitude for the hospitality at the European Space Astronomy Centre (ESAC) during the course of this work. We thank the XMM-Newton Science Operations Centre (SOC) for technical advice and especially Matteo Guainazzi for his continuous support. The near infrared data were provided by the Kanata TRISPEC team prior to publication, while the optical data were taken from the AAVSO International Database and the VSOLJ Observation Database contributed by observers worldwide.

This research has made use of data obtained from Data ARchives and Transmission System (DARTS), provided by the Center for Science-satellite Operation and Data Archives (C-SODA) at the Institute of Space and Astronautical Science (ISAS) of Japan Aerospace Exploration Agency (JAXA), the High Energy Astrophysics Science Archive Research Center (HEASARC), provided by the National Aeronautics and Space Administration (NASA) Goddard Space Flight Center (GSFC), and of the SIMBAD database, operated at CDS, Strasbourg, France.

D.T. is financially supported by the Japan Society for the Promotion of Science (JSPS). J.J.D. was supported by the NASA contract NAS8-39073 to the Chandra X-ray Observatory Center (CXC). J.P.O. acknowledges the support of the Science and Technology Facilities Council (STFC).

References

- Anders, E. & Grevesse, N. 1989, *Geochim. Cosmochim. Acta*, 53, 197
- Ashok, N. M., Banerjee, D. P. K., Joshi, V., et al. 2008, *Central Bureau Electronic Telegrams*, 1354, 1
- Balman, S., Orio, M., & Ogelman, H. 1995, *ApJ*, 449, L47
- Barthelmy, S. D., Barbier, L. M., Cummings, J. R., et al. 2005, *Space Science Reviews*, 120, 143
- Baskill, D. S., Wheatley, P. J., & Osborne, J. P. 2005, *MNRAS*, 357, 626
- Bode, M. F. & Evans, A. 2008, *Classical Novae*, ed. Bode, M. F. & Evans, A. (Cambridge: Cambridge University Press)
- Bode, M. F., O'Brien, T. J., Osborne, J. P., et al. 2006, *ApJ*, 652, 629
- Burrows, D. N., Hill, J. E., Nousek, J. A., et al. 2005, *Space Science Reviews*, 120, 165
- Byckling, K., Mukai, K., Thorstensen, J. R., & Osborne, J. P. 2010, *MNRAS*, 408, 2298
- Channugam, G., Ray, A., & Singh, K. P. 1991, *ApJ*, 375, 600
- Cordova, F. A., Jensen, K. A., & Nugent, J. J. 1981, *MNRAS*, 196, 1
- Cropper, M. 1990, *Space Sci. Rev.*, 54, 195
- della Valle, M. & Livio, M. 1995, *ApJ*, 452, 704
- den Herder, J. W., Brinkman, A. C., Kahn, S. M., et al. 2001, *A&A*, 365, L7
- Downes, R. A. & Duerbeck, H. W. 2000, *AJ*, 120, 2007
- Drake, J. J., Ercolano, B., & Swartz, D. A. 2008, *ApJ*, 678, 385
- Drake, J. J. & Orlando, S. 2010, *ApJL*, 720, L195
- Drechsel, H., Rahe, J., Wargau, W., Seward, F. D., & Wang, Z. R. 1983, *A&A*, 126, 357
- Ezuka, H. & Ishida, M. 1999, *ApJ*, 120, S277
- Frank, J., King, A., & Raine, D. 1992, *Accretion power in astrophysics*, ed. Frank, J., King, A., & Raine, D.
- Friedjung, M. 1987, *A&A*, 180, 155
- Gehrels, N., Chincarini, G., Giommi, P., et al. 2004, *ApJ*, 611, 1005
- George, I. M. & Fabian, A. C. 1991, *MNRAS*, 249, 352
- Guainazzi, M., Kirsch, M., F., H., & de Juan Ovelar, M. 2010, *Evaluation of the spectral calibration accuracy in EPIC-pn fast modes, version 1.2*
- Hellier, C. & Mukai, K. 2004, *MNRAS*, 352, 1037
- Helton, L. A., Woodward, C. E., Vanlandingham, K., & Schwarz, G. J. 2008, *Central Bureau Electronic Telegrams*, 1379, 1
- Hernanz, M. & Sala, G. 2002, *Science*, 298, 393
- Hubble, E. P. & Duncan, J. C. 1927, *ApJ*, 66, 59
- Hyodo, Y., Tsujimoto, M., Hamaguchi, K., et al. 2008, *PASJ*, 60, S85
- Ibarra, A. & Kuulkers, E. 2008, *The Astronomer's Telegram*, 1473, 1
- Ibarra, A., Kuulkers, E., Beardmore, A., et al. 2008, *The Astronomer's Telegram*, 1478, 1
- Ibarra, A., Kuulkers, E., Osborne, J. P., et al. 2009, *A&A*, 497, L5
- Ishida, M., Silber, A., Bradt, H. V., et al. 1991, *ApJ*, 367, 270
- Ishisaki, Y., Maeda, Y., Fujimoto, R., et al. 2007, *PASJ*, 59, S113
- Jansen, F., Lumb, D., Altieri, B., et al. 2001, *A&A*, 365, L1
- Kokubun, M., Makishima, K., Takahashi, T., et al. 2007, *PASJ*, 59, S53
- Koyama, K., Tsunemi, H., Dotani, T., et al. 2007, *PASJ*, 59, S23
- Kuulkers, E., Ibarra, A., Page, K. L., et al. 2008, *The Astronomer's Telegram*, 1480, 1
- Liller, W. & Jones, A. 1999, *Information Bulletin on Variable Stars*, 4774, 1
- Lloyd, H. M., O'Brien, T. J., Bode, M. F., et al. 1992, *Nature*, 356, 222
- Lynch, D. K., Russell, R. W., Rudy, R. J., Woodward, C. E., & Schwarz, G. J. 2008, *IAU Circ.*, 8935, 1
- Mason, K. O., Breeveld, A., Much, R., et al. 2001, *A&A*, 365, L36
- Maughan, B. J., Jones, L. R., Ebeling, H., & Scharf, C. 2004, *MNRAS*, 351, 1193
- Mitsuda, K., Bautz, M., Inoue, H., et al. 2007, *PASJ*, 59, S1
- Mukai, K. & Ishida, M. 2001, *ApJ*, 551, 1024
- Mukai, K. & Orio, M. 2005, *ApJ*, 622, 602
- Mukai, K. & Shiokawa, K. 1993, *ApJ*, 418, 863
- Mukerjee, K., Osborne, J. P., Wells, A. A., et al. 2004, in *Society of Photo-Optical Instrumentation Engineers (SPIE) Conference Series*, Vol. 5165, *Society of Photo-Optical Instrumentation Engineers (SPIE) Conference Series*, ed. K. A. Flanagan & O. H. W. Siegmund, 251–261
- Nakajima, H., Yamaguchi, H., Matsumoto, H., et al. 2008, *PASJ*, 60, 1
- Nakano, S., Beize, J., Jin, Z., et al. 2008, *IAU Circ.*, 8934, 1

- Nelson, T., Orio, M., Cassinelli, J. P., et al. 2008, *ApJ*, 673, 1067
- Ness, J.-U. 2010, *Astronomische Nachrichten*, 331, 179
- Ness, J.-U., Drake, J. J., Beardmore, A. P., et al. 2009, *AJ*, 137, 4160
- Ness, J.-U., Osborne, J. P., Dobrotka, A., et al. 2011, *MNRAS*, submitted.
- Ness, J.-U., Starrfield, S., Gonzalez, R., et al. 2008a, *The Astronomer's Telegram*, 1561, 1
- Ness, J.-U., Starrfield, S., Gonzalez, R., et al. 2008b, *The Astronomer's Telegram*, 1573, 1
- Norton, A. J. & Mukai, K. 2007, *A&A*, 472, 225
- Norton, A. J. & Watson, M. G. 1989, *MNRAS*, 237, 715
- Orio, M., Mukai, K., Bianchini, A., de Martino, D., & Howell, S. 2009, *ApJ*, 690, 1753
- Orio, M., Parmar, A., Benjamin, R., et al. 2001, *MNRAS*, 326, L13
- Osborne, J. P., Page, K., Evans, P., et al. 2008, *The Astronomer's Telegram*, 1542, 1
- Osborne, J. P., Page, K. L., Beardmore, A. P., et al. 2011, *ApJ*, submitted.
- Page, K. L., Osborne, J. P., Evans, P. A., et al. 2008, *The Astronomer's Telegram*, 1523, 1
- Page, K. L., Osborne, J. P., Evans, P. A., et al. 2010, *MNRAS*, 401, 121
- Page, K. L., Osborne, J. P., Read, A. M., et al. 2009, *A&A*, 507, 923
- Pagnotta, A., Schaefer, B. E., Xiao, L., Collazzi, A. C., & Kroll, P. 2009, *AJ*, 138, 1230
- Patterson, J. 1994, *PASP*, 106, 209
- Payne-Gaposchkin, C. 1957, *The Galactic Novae*, ed. C. Payne-Gaposchkin
- Prialnik, D. 1986, *ApJ*, 310, 222
- Prialnik, D. & Kovetz, A. 1995, *ApJ*, 445, 789
- Prialnik, D., Livio, M., Shaviv, G., & Kovetz, A. 1982, *ApJ*, 257, 312
- Prialnik, D. & Shara, M. M. 1986, *ApJ*, 311, 172
- Ribeiro, F. M. A. & Diaz, M. P. 2008, *PASJ*, 60, 327
- Roming, P. W. A., Kennedy, T. E., Mason, K. O., et al. 2005, *Space Science Reviews*, 120, 95
- Rothenflug, R. & Arnaud, M. 1985, *A&A*, 144, 431
- Rudy, R. J., Lynch, D. K., Russell, R. W., Woodward, C. E., & Covey, K. 2008, *IAU Circ.*, 8938, 2
- Samus, N. N. 2008, *IAU Circ.*, 8934, 2
- Saxton, R. D., Read, A. M., Esquej, P., et al. 2008, *VizieR Online Data Catalog*, 348, 611
- Schaefer, B. E. 2010, *ApJ*, 187, S275
- Schaefer, B. E. & Collazzi, A. C. 2010, *AJ*, 139, 1831
- Serlemitsos, P. J., Soong, Y., Chan, K., et al. 2007, *PASJ*, 59, S9
- Shara, M. M., Livio, M., Moffat, A. F. J., & Orio, M. 1986, *ApJ*, 311, 163
- Smith, R. K., Brickhouse, N. S., Liedahl, D. A., & Raymond, J. C. 2001, *ApJ*, 556, L91
- Sokoloski, J. L., Luna, G. J. M., Mukai, K., & Kenyon, S. J. 2006, *Nature*, 442, 276
- Starrfield, J. H., Illiadis, C., & Hix, W. R. 2008, in *Classical Novae*, ed. M. Bode and A. Evans (Cambridge: Cambridge University Press), 77–101
- Strüder, L., Briel, U., Dennerl, K., et al. 2001, *A&A*, 365, L18
- Takahashi, T., Abe, K., Endo, M., et al. 2007, *PASJ*, 59, S35
- Takei, D., Tsujimoto, M., Kitamoto, S., et al. 2009, *ApJ*, 697, L54
- Talavera, A. 2009, *Ap&SS*, 320, 177
- Tomov, T., Mikolajewski, M., Brozek, T., et al. 2008a, *The Astronomer's Telegram*, 1485, 1
- Tomov, T., Mikolajewski, M., Ragan, E., Swierczynski, E., & Wychudzki, P. 2008b, *The Astronomer's Telegram*, 1475, 1
- Tsujimoto, M., Feigelson, E. D., Grosso, N., et al. 2005, *ApJ*, 160, S503
- Tsujimoto, M., Takei, D., Drake, J. J., Ness, J.-U., & Kitamoto, S. 2009, *PASJ*, 61, S69
- Turner, M. J. L., Abbey, A., Arnaud, M., et al. 2001, *A&A*, 365, L27
- Voges, W., Aschenbach, B., Boller, T., et al. 2000, *VizieR Online Data Catalog*, 9029, 0
- Warner, B. 2003, *Cataclysmic Variable Stars*, ed. Warner, B. (Cambridge: Cambridge University Press)
- Warner, B. 2008, in *Classical Novae*, ed. Bode, M. F. & Evans, A. (Cambridge: Cambridge University Press), 16–33
- Wilms, J., Allen, A., & McCray, R. 2000, *ApJ*, 542, 914